FEATURE ARTICLE

Molecular Assembly in Ordered Mesoporosity: A New Class of Highly Functional Nanoscale Materials

Jun Liu,* Yongsoon Shin, Zimin Nie, Jeong Ho Chang, Li-Qiong Wang, Glen E. Fryxell, William D. Samuels, and Gregory J. Exarhos

Pacific Northwest National Laboratory, Richland, Washington 99352

Received: March 15, 2000; In Final Form: June 29, 2000

Assembly of organized molecular structures in ordered mesoporosity has shown to be a very powerful approach to synthesize novel functional nanoscale materials. This approach allows rational design of a wide range of material properties, such as pore dimension, surface chemistry, stereochemistry, spatial distribution of functionality, etc. This paper discusses molecular conformations and assembly mechanisms and illustrates the principles involved in fabricating sophisticated molecular structures in the pore channels. First, an introduction highlights the important progress in synthesizing and understanding ordered mesoporous materials and in incorporating functional molecules and groups in these mesoporous materials. Next, the molecular conformations of simple alkyl chains are discussed as related to chain lengths and pore geometry. The pore size, as well as the uniformity of the porosity, can affect how the long-chain molecules are assembled. Homogeneous molecular layers can be formed in 10 nm pores. Smaller pore sizes cause pore clogging and chain entanglement. Larger pore sizes increase the degree of pore irregularity and produce disordered multilayer coating. Molecules with intermediate chain lengths form better molecular layer structures. Detailed mechanisms of monolayer formation are studied, and a stepwise growth model is proposed. The step-growth mechanism is due to the surface roughness of the pore channels and is believed to be universal in forming "monolayers" involving surfaces that are not atomically smooth. Finally, the development of multifunctional nanoporous materials is described. Examples include multifunctionalized catalysts, hierarchical size-and-shape selective nanoporous materials with tunable micropatterns and microcavities. The assembly of multifunctional groups and structures will allow us to develop sophisticated nanoscale materials with "enzyme mimic" and "biomimic" properties.

Introduction: Ordered Mesoporous Materials and Molecular Assembly in Mesoporosity

The discovery of ordered mesoporous materials using a surfactant-templated approach has opened a new era in the synthesis of ordered nanoscale materials.[1] This class of materials has attracted the attention of scientists from many different fields because of some of its unique features. First, the material is synthesized using a self-assembly approach: surfactant molecules co-assemble with the inorganic materials into sophisticated nanoscale structures through favorable molecular interactions.[2] This synthetic approach is a drastic departure from traditional materials processing in which different components are mixed and forced together by applying high heat or high pressure. Second, the resultant nanoscale materials have a delicate structural ordering that is very difficult to achieve using traditional synthetic routes. Not only can the scale of ordering (from 1.5 to 30 nm) and the crystalline symmetry (hexagonal, lamella, cubic, etc.) be controlled but also the morphology on the macroscopic scales can be tailored.

Since 1992, mesoporous materials research has become a very active area because of its great potential. Numerous papers have been published on the preparation of mesoporous materials of novel chemical compositions and on the fundamental understanding of the reaction processes.[3] A wide range of mesoporous materials has been prepared,[4] including alumina, zirconia, titania, niobia, tantalum oxide, manganese oxide,[5] and even metals.[6] In general, direct ionic interaction,[1] mediated ionic interaction,[7] and neutral hydrogen bonding[8,9] can be used. A nonaqueous process was also used to assemble ordered germanium sulfides from $(Ge_4S_{10})^{4-}$ clusters.[10] Besides traditional surfactants, block copolymers have also been used as templates.[11,12] The block copolymer directed synthesis greatly expanded the pore size and compositional range of mesoporous materials.

The development of different forms of mesoporous materials has also attracted wide attention. Recently, progress has been made in fabricating oriented mesoporous films on various substrates[13,14] and in making free-standing films,[15] spheres,[16,17] fibers,[18,19] and single crystalline mesoporous materials in which all the pore channels are aligned.[20] Mesoporous silica films using a rapid evaporation approach (dip coating[21,22] or spin coating[23]) have been considered prime candidates for ultralow dielectric interlayer structures in next-generation microelectronic devices. A magnetic field has been used to align the pore channels before the silicate was polymerized.[24] In addition, a wide range of

* To whom correspondence should be addressed.

10.1021/jp0009812 CCC: $19.00
Published on Web 08/09/2000

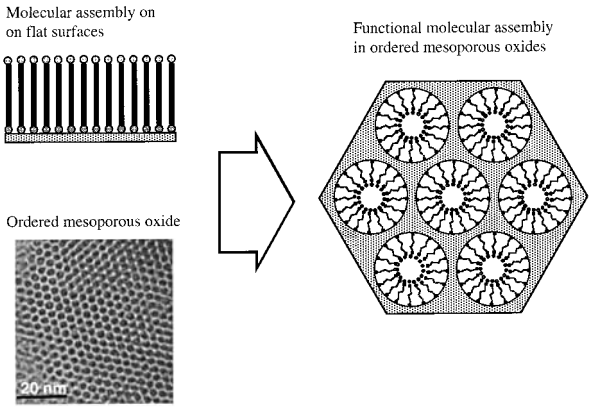

Figure 1. Assembly of molecular monolayers in ordered mesoporous materials (from ref 36b with permission). Copyright 1998 Wiley-VCH.

intrigue morphologies and patterns have been reported, including spiral and toroidal shapes,[25] and silica vesicles.[26] Hierarchically ordered nanoscale patterns were generated by combining multiscale templating and micromolding, or lithography.[27] These patterns will have potential as novel optical waveguides.[28] Biogenic or biomimetic directing agents (copolypeptides) can also be used to control the morphologies and shapes.[29]

Mesoporous silica has been doped with elements possessing catalytic properties[30] and with conducting polymers.[31] Ordered ruthenium clusters were introduced to the mesoporous channels.[32] The mesoporous channels can also function as nanoextruders to produce liner polyethylene nanofibers of high molecular weight.[33] Recently, mesoporous framework structures containing bridge-bonded ethene (and other) organic groups were reported.[34] These types of materials raise the possibility of generating integrated organic−inorganic hybrid materials.

The successful synthesis of ordered mesoporous materials has wide scientific and practical implications. These materials have a very high surface area (>1000 m^2/g), ordered pore structure (mostly hexagonal packed cylindrical pore channels), and extremely narrow pore-size distribution. The ordered and uniform pore geometry provides an ideal platform to perform a wide range of chemical processes.

The purpose of this paper is to discuss the assembly of molecular layer structures and functional groups in mesoporous channels. This approach has led to the development of a class of hybrid nanoscale material that has demonstrated great potential for many applications, such as adsorption, ion exchange, catalysis, and sensing. The assembly of molecular structures in mesoporosity provides a unique opportunity to rationally engineer the surface properties. For example, hybrid mesoporous materials with functional molecules already demonstrate exceptional selectivity and capacity for adsorbing heavy metal ions from contaminated waste streams.[35,36] Besides heavy metals, more efficient materials have also been developed for remediation involving anions such as chromate and arsenate[37] and radionuclides.[38]

The assembly of functional molecules and groups in mesoporous channels draws an analogy from the preparation of self-assembled monolayers on flat substrates (Figure 1). Several approaches have been used to incorporate functional groups and molecules into mesoporous materials, mostly for catalytic applications.[39] These studies have been extensively reviewed by Möller and Bein.[40] The most straightforward method involves direct silanation of partially hydroxylated mesoporous silica, which depends on the population density of hydroxyl groups existing on the surface.[41] The hydroxylation problem can be partially solved by using uncalcined mesoporous silica, which was prepared using a neutral surfactant. The surfactant was subsequently removed by solvent-extraction techniques.[35] High density molecular monolayers can be constructed by purposely introducing physically adsorbed layers of water molecules before silanation.[36] Alternatively, co-condensation is a one-step process in which the functional molecules are incorporated into the materials while the mesoporous materials are being prepared.[42,43]

In general, the novel hybrid porous materials containing functional molecules and monolayers allow us to tailor the pore size and surface chemistry on a molecular scale. Key material parameters can be adjusted and independently evaluated, including the following.

(1) Pore Channel Size. The actual pore channel spacing is determined by the pore size of the support and the chain length of functional molecules on the surface. Therefore, the pore channel sizes will vary from ångström level to nanometer scale by adjusting the pore size of the support and the molecular size of the functional groups.

(2) Stereochemical Interactions. This stereochemical relationship can be adjusted by manipulating the arrangement of the functional groups on the surface (for example, the population density or chain length).

(3) Functionality of the Surface Groups. The functional groups, as well as their spatial distribution, can be substituted and tailored for a particular application.

Molecular Conformation in Nanoporosity

The assembly of molecular structures and monolayers on flat substrates has been studied for a long time. Molecular monolayers are widely explored for engineering the surface and interfacial properties of materials such as wetting, adhesion, and friction.[44] These monolayers are also used to mediate the molecular recognition processes and to direct oriented crystal growth.[45] Chemical and physical modification of solid surfaces is extensively used in chromatography, chemical analysis, catalysis, electrochemistry, and electronic industry. Molecular monolayers are also widely investigated as an effective means to fabricate novel sensing and electronic devices. The molecular arrangement and the chain conformation on flat substrates have been extensively studied by atomic force microscopy (AFM), contact angle measurement, small angle scattering, and many other techniques.[44]

Compared to flat substrates, the geometry of the mesoporosity is unique. Many factors can affect the formation of the molecular structures, including: (1) the pore sizes, (2) the chain lengths, (3) the pore shapes, and (4) the degree of uniformity of the pores. Fortunately, the high surface area makes it possible to use spectroscopy techniques such as nuclear magnetic resonance (NMR) to interrogate the chain conformation and chain mobility. The uniform pore geometry allows us to accurately measure the pore sizes, from which information regarding the chain arrangement can be inferred.

In this study, mesoporous materials with four different pore diameters were used: 3.2, 9.3, 17, and 30 nm. They are referred to as 3 nm, 10 nm, 17 nm, and 30 nm mesoporous materials hereafter for simplicity. The 3 nm mesoporous material was prepared according to the procedure reported by Beck et al.,[1] and large-pore mesoporous materials were prepared according to the procedure reported by Yang et al.[11,12]

Figure 2 shows the transmission electron microscopy (TEM) micrographs of the four mesoporous materials: (a) 3 nm, (b) 10 nm, (c) 17 nm, and (d) 30 nm. The 3 nm and 10 nm materials have uniform and ordered cylindrical pore channels. The 17 nm material has some degree of ordering, but the morphology

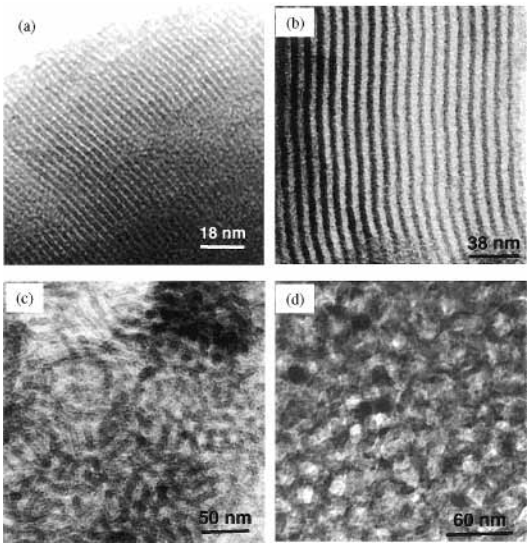

Figure 2. TEM micrographs of 3 nm (a), 10 nm (b), 17 nm (c), and 30 nm (d) mesoporous materials.

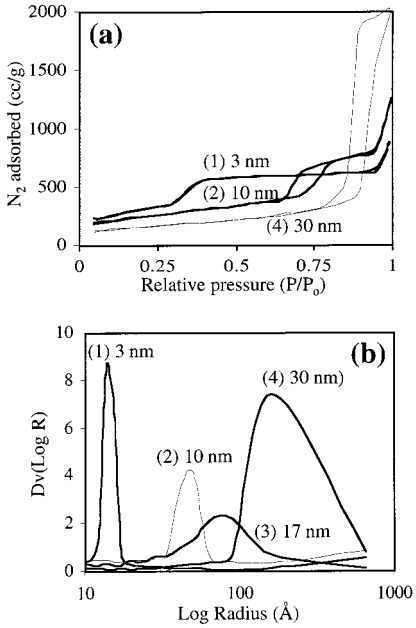

Figure 3. (a) N_2 adsorption isotherms and (b) pore-size distributions of 3 nm, 10 nm, 17 nm, and 30 nm mesoporous materials. The adospriton isotherm for Sample 3 (17 nm) is not shown in Figure 3a for clarity.

is much more disordered. The porosities in the 30 nm material are almost completely disordered, but the pore sizes are more or less uniform. Each cell is about 30 nm in diameter. A Quantachrome nitrogen adsorption instrument was used to measure the surface area and pore size. The pore-size distributions were obtained from the adsorption branches using the standard Barrett−Joyner−Halenda (BJH) method without further correction.[46] The adsorption branch was found to give representative results about the pore-size distribution of ordered mesoporous materials when a corrected Kevin equation is used.[47,48] The surface area and the pore-size distributions reported in this paper only gave a relative estimate of the changes in these quantities. More detailed pore-structure analysis is underway and will be published separately.

Figure 3 shows N_2 adsorption isotherms and the pore-size distributions of the four materials. The N_2 adsorption isotherms are typical of uniform pore channels with wide and narrow pore

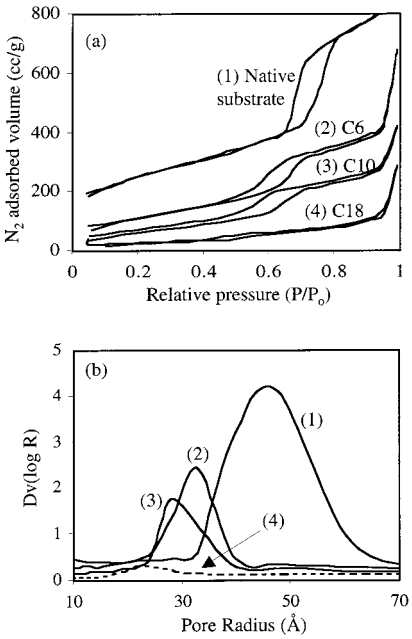

Figure 4. (a) N_2 adsorption isotherms and (b) pore-size distributions of 10 nm materials after C6, C10, and C18 chains were deposited.

regions in the pore channels. The widened hysteresis with increased pore sizes are attributed to the increased pore-size variations in the large-pore materials. The narrow pore parts have a strong influence on the desorption branches.[47]

Alkyltrialkoxysilane molecules of different chain lengths ($(CH_3O)_3Si(CH_2)_{n-1}CH_3$, $n = 6$, 10, 18, hereafter referred to as C6, C10, C18) were deposited in the porous substrates according to the procedure we published earlier.[36] After the alkyl chains were deposited in the mesoporous materials, the pore diameters were reduced, depending on the chain length. The pore-size changes as related to the chain (or ligand) sizes were previously reported by Antochshuk and Jaroniec.[49] Figure 4 shows the pore-size distributions (from adsorption branch) of the 10 nm materials when alkylsilane molecules of different chain lengths were deposited, and Table 1 lists the pore sizes and surface areas of different materials after molecules of different chain lengths were deposited in the porosity. On the basis of the chain length, we can estimate the expected remaining pore sizes. As seen from Table 1, the 3 nm pores were partially clogged by C6 and completely clogged by C10 and C18. For the 10 nm pores, the pore radii were reduced by 16 Å with C6, 20 Å for C10, and 27 Å for C18. The chain lengths for C6, C10, and C18 can be estimated to be about 12, 17, and 27 Å, respectively. The changes in pore sizes are consistent with the chain lengths. In our experiments, the alkylsilane molecules were deposited in a refluxing condition in toluene with the addition of a very small amount of water to achieve high surface coverage and a high degree of cross-linking. Therefore, we expect the molecular chains to have mixed gauche and train conformation. We also expect some degree of "vertical" polymerization, as discussed by Fatumbi et al.[50]

However, for pore sizes larger than 10 nm, the pore sizes were reduced by more than the chain length, especially for the 30 nm samples (the pore radii were reduced by 60 Å). In addition, the pore-size change in the 30 nm porosity is independent of the chain length. This suggests that the molecular chains in the large-pore channels have very disordered multilayer structures. The molecular layer thickness is not controlled by the chain length.

TABLE 1: Surface Areas and Pore Sizes as a Function of Initial Pore Sizes and Chain Lengths

	3 nm SiO_2		10 nm SiO_2		17 nm SiO_2		30 nm SiO_2	
	S_{BET} (m^2/g)	D_{ad} (Å)	S_{BET} (m^2/g)	D_{ad} (Å)	S_{BET} (m^2/g)	D_{ad} (Å)	S_{BET} (m^2/g)	D_{ad} (Å)
native SiO_2	1000	32	911	93	661	170	533	300
C_6	377	17	421	65	510	128	381	177
C_{10}	99	NA	253	56	268	123	276	175
C_{18}	38	NA	96	43	269	120	276	175

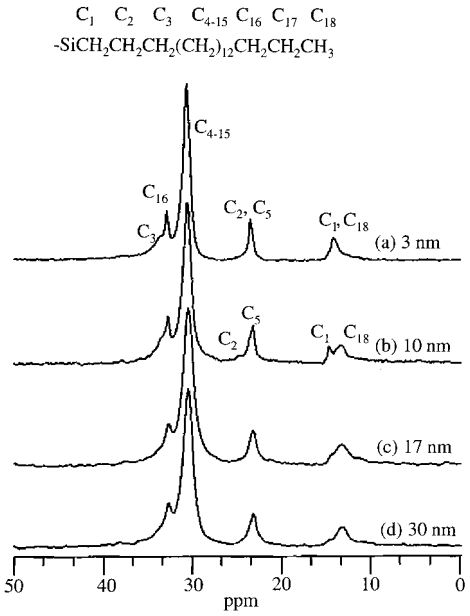

Figure 5. Single pulse (SP) ^{13}C NMR spectra of C18 molecules in 3 nm, 10 nm, 17 nm, and 30 nm pores. The C_1 and C_{18} peaks change systematically with pore size, depending on the molecular conformation.

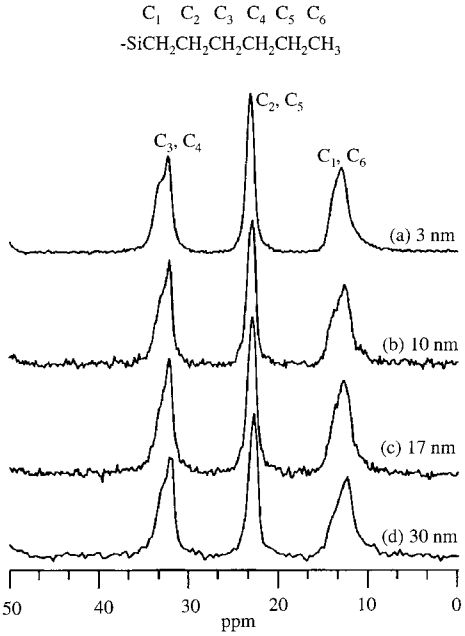

Figure 6. Single pulse (SP) ^{13}C NMR spectra of C6 molecules in 3 nm, 10 nm, 17 nm, and 30 nm pores. The spectra are essentially the same.

^{13}C and ^{29}Si solid-state nuclear magnetic resonance (NMR) spectra were obtained.[51] Single pulse (SP) magic angle spinning (MAS) ^{13}C NMR spectra along with the peak assignment are given in Figure 5 for C18 on mesoporous silica with pore sizes of 3, 10, 17, and 30 nm, respectively. The peak assignment was based on previous studies.[48,50] Several features of the ^{13}C NMR spectra of alkylsilanes on silica are noteworthy in Figure 5. Spectra for C18 on mesoporous silica with different pore sizes (see Figures 5a−d) appear to be similar, except the resonance features between 12 and 15 ppm. The largest resonance at 30.6 ppm is associated with the internal methylenes (C4−15). On the basis of the chemical shift position, the alkyl chain has adopted mixed gauche and trans conformations independent of pore sizes, as expected from the synthesis conditions. Figure 5b for C18 on a 10 nm pore shows two well-resolved resonance peaks at 14.7 and 13.4 ppm, which correspond to the two terminal carbon atoms, C_1 methylene next to the Si and C_{18} carbon of the methyl group at the end of the chain. However, these two peaks become less resolved with increased pore size. For C18 on 30 nm pores, these two peaks almost merge into one peak at 13.1 ppm. As the pore size decreases from 10 to 3 nm, these two resonance peaks coalesce into one peak at about 14.2 ppm. The same trend was also observed for C10 on mesoporous silica with different pore sizes. For C6, the ^{13}C NMR spectra are similar for all pore sizes (Figure 6).

Since the resonances at 12−15 ppm are associated with first carbon (C_1) and last carbon (C_{18}) corresponding to the two ends of the alkylsilane chains, the chemical shift of those carbon groups should be sensitive to the conformational arrangement of the terminal alkyl groups with respect to the other alkyl chains and to the silica surface. The changes in chemical shift associated with the C_1 and C_{18} carbon groups indicate that the alkylsilanes are arranged differently in silica with different pore sizes. In the 3 nm pore, the terminal groups of the long chains are most likely entangled and constrained. The steric crowding effect on the terminal groups could cause the C peak corresponding to the methyl group to downshift by more than 1 ppm.[52] In 10 nm pores, the molecular chains are more organized, giving rise to well-resolved peaks for C_1 and C_{18} carbon. In 17 nm and 30 nm pores, the molecules are stacked together as a completely disordered multilayer, so the C_1 peak was broadened and not obvious. The ^{13}C NMR results are in agreement with results obtained from nitrogen adsorption studies, which suggest different conformations associated with the different pore size of silica. On the other hand, C6 molecules are smaller than the pore diameter, and the effect of pore constraint was not observed for C6.

The possible chain conformations based on the nitrogen adsorption and NMR results in different pore geometries are illustrated in Figure 7.

^{29}Si NMR spectra were also obtained to further illustrate the chemical environments of the interfacial region. Figure 8 shows the spectra for different chain lengths in 10 nm porosity. The peaks from −40 to −80 ppm correspond to the siloxane groups.[36] It is interesting that C10 chains show a higher degree of cross-linking than C6 chains. For C6, the cross-linking ratio, Si(cross-link)/Si(terminal), is about 0.77. This ratio increased to 1.23 for C10 and decreased to 0.48 for C18. The driving force to form a molecular monolayer includes the intermolecular chain-to-chain attraction and the condensation reaction between the alkylsilane molecules and the substrate. For C6, the chain-to-chain interaction is weak because of the short chain length. Therefore, the molecules are not closely packed. Increased chain

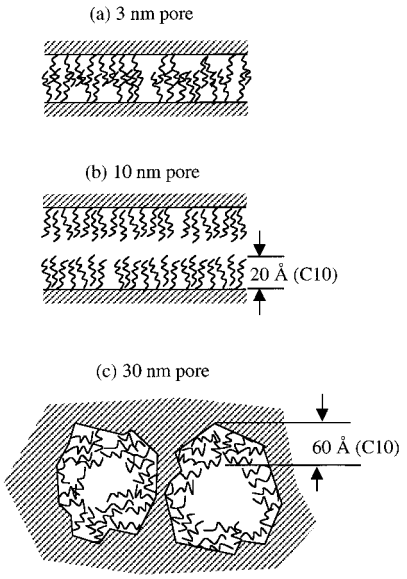

Figure 7. Suggested molecular conformations in 3 nm, 10 nm, and 30 nm pores based on NMR and N_2 adsorption studies.

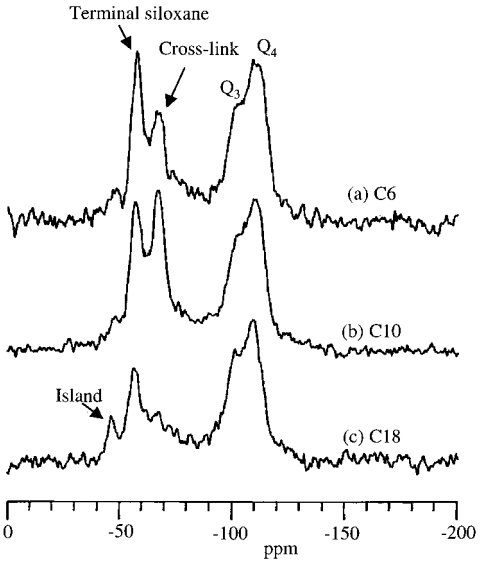

Figure 8. ^{29}Si NMR spectra of C6, C10, and C18 molecules 10 nm pores. C18 chains have the lowest degree of cross-linking due to the steric hindrance.

length for C10 increases the chain-to-chain attraction, therefore accounting for the efficiency of packing and cross-linking. However, a further increase of chain length to C18 reduced the efficiency of packing because the steric effect of the long chains prevents effect packing in the porous channels.

In addition to chain length, the pore size also has an effect on the cross-link density, as shown in Figure 9. For C6, the cross-linking ratio is about 0.48 for both 3 nm and 30 nm pores. This ratio is slightly higher in 10 nm pores (about 0.67). For C10 and C18, the increased degree of cross-linking is more evident for the 10 nm pores. For example, for C10, the cross-linking ratio is about 0.77 for 30 nm pores, which increases to 1.23 for 10 nm pores and decreases to 0.95 for 3 nm pores. These results are consistent with the molecular conformations drawn in Figure 7.

Molecular Mechanisms of Monolayer Formation

Since the formation of molecular monolayers plays such an important role for many applications, the mechanisms of monolayer formation have been widely investigated. The formation of molecular monolayers involving silane molecules of different chain lengths on smooth surfaces, silica spheres, and gels has been extensively studied. Kinetically, several steps have been reported:[53] (1) rapid reaction of silane molecules with residual or adsorbed water to form hydrolyzed monomers or oligomers, and aggregation of such monomers and oligomers, (2) Diffusion and adsorption of the silane monomers and oligomers onto the substrates, and (3) chemical adsorption to the surface, elimination of water, and the formation of the Si−O−Si bonds with the substrate. Island and domain structures are widely observed. Maoz and Sagiv[54] reported that dense molecular arrays will form if the adsorption is carried out from solutions above certain critical concentrations. Less-dense arrays will be formed when adsorption is carried out in solutions below the critical concentration. A fractal growth model was proposed by Schwartz et al., to account for the self-similar domain structures formed at different times of reaction.[55] Many factors, such as the amount of water, reaction temperature, particle size, and the use of different solvents, are found to affect the monolayer formation.

Hybrid mesoporous materials involve the formation of molecular monolayers in confined spaces, with dimensions approaching the sizes of the silane molecules. There have been few reports on the mechanisms in such systems so far. Here, we report the formation of molecular monolayers in tailored mesoporous substrates as a function of surface coverage.

The mesoporous substrate contains uniform cylindrical pore channels with wide and narrow regions. Such uniform mesoporous materials provide ideal substrates to quantitatively study the monolayer chemistry. For the first time in our research, we provide direct evidence of a new step-growth mechanism in which the silane molecules are first deposited in the wide region. When the wide pore region is filled, the silane molecules begin to deposit in the narrow pore region. After the narrow pore region is filled, the silane molecules begin to deposit in the wide pore region as second layers. The pore size in the wide region and narrow region change alternatively and discretely in accordance with this step-growth mechanism and the molecular size of the silane. We also believe that this step-growth model is universal and has implications for monolayer chemistry with different substrates. In reality, atomically smooth substrates are seldom encountered. Most substrates contain surface roughness in the form of holes, trenches, steps, etc. Geometrically, the wide regions in the pore channel are similar to a concave defect on the surface (such as a hole). The mechanism suggests that on a rough surface, the silane molecules would be deposited on the concave regions first and then spread to the neighboring surfaces. After the first layers are filled, the second layer will start to build up in the concave region again.

First, TEM images were obtained of the native 10 nm mesoporous substrate (Figure 10). This material has a hexagonal structure, and the TEM images were obtained parallel to the direction of the pore channels under slightly underfocused conditions. In general, the pore channels are ordered, and the pore sizes are quite uniform. However, a close examination of the pore-wall structure indicates that the pore surface is not atomically smooth. As a result, the pore diameters along the pore channels can change by several nanometers. Figure 10a is the regular image with the dark contrast representing the silica walls. In the inverted contrast image (Figure 10b), the dark contrast represents the pore channels, and the white contrast represents the silica walls. The surface roughness revealed in

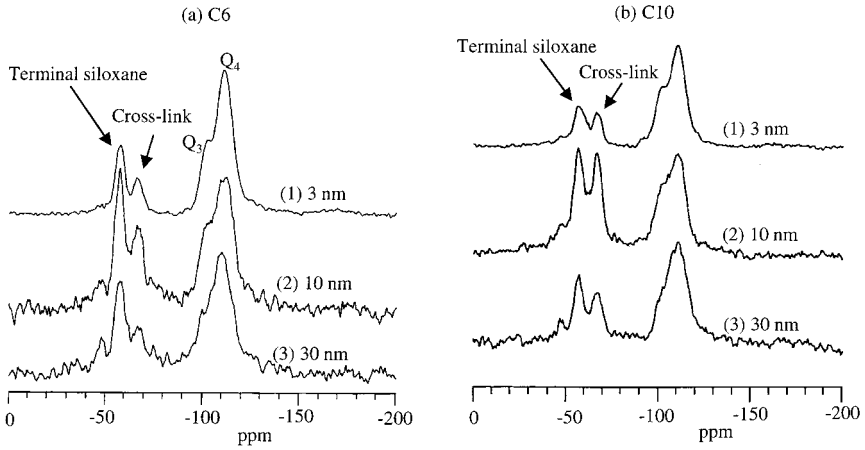

Figure 9. ^{29}Si NMR spectra of (a) C6 chains in 3 nm, 10 nm, and 30 nm pores, and (b) C10 chains in 3 nm, 10 nm, and 30 nm pores. The cross-linking for C6 is similar in all pores, but different for C10. The 10 nm pores give the highest degree of cross-linking.

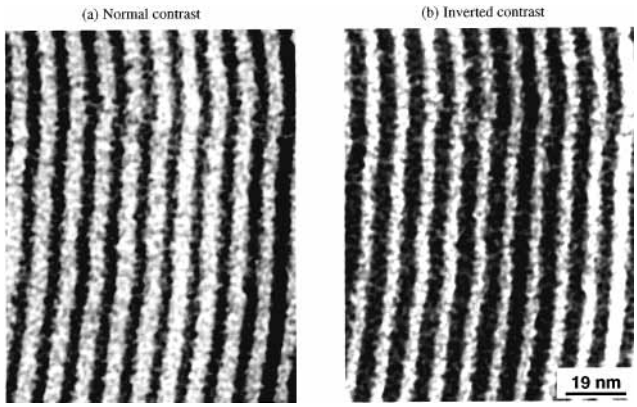

Figure 10. High magnification TEM micrographs of 9.3 nm materials, showing the rough wall surfaces. (a) Normal contrast. The dark region is the silica, and the white region is the pore. (b) Inverted contrast. The dark region is the pore, and the white region is the silica.

TABLE 2: Pore Sizes as a Function of APS Coverage

APS (mmol/g SiO_2)	D_{ad} (Å)	D_{de} (Å)
0	93	65
1.6	78	65
3.3	78	55
4.6	65	56
5.7	55	50
7.2	56	50

the TEM images is consistent with the nitrogen adsorption studies, which show wide and narrow pore regions in the channels.

The N_2 adsorption and desorption isotherms, together with the pore-size distributions and different surface coverages of aminopropyltrimethoxysilanes (APS), are shown in Figure 11. As discussed earlier, the adsorption branches give the pore size of the wide pore regions.[47] As the silane molecules were deposited on the substrate, the surface area and the pore size were reduced. However, it is interesting to notice two important observations (Table 2). First, the pore size does not change continuously with increasing surface coverage. Instead, it only changes in steps. Below 45% (3.3 mmol APS/g SiO_2) surface coverage (the percentage of the surface coverage was calculated based on the available silanol groups),[36] the pore diameters from the adsorption branch were reduced from 93 to 78 Å and stayed constant in this range. At 60% surface coverage (4.6 mmol APS/g SiO_2), the pore diameter from the adsorption branch was reduced to 65 Å. A surface coverage higher than 60% gave a pore diameter of 55 Å. Second, the change in the pore diameter from the desorption branch also occurs in steps and is always behind the pore-diameter change from the adsorption branch. Below 20% surface coverage (1.5 mmol APS/g SiO_2), the pore diameter from the desorption branch was not changed at all. From 20% to 60% (4.6 mmol APS/g SiO_2) surface coverage, the desorption pore diameter was reduced to 55 Å. More than 60% surface coverage gave a desorption pore diameter of 50 Å.

The implication of the pore-diameter change as a function of surface coverage is clear because the adsorption branch gives the pore diameter of the wide pore region, and the desorption branch gives information on the narrow pore region. The most reasonable explanation is that the silane molecules were first deposited in the wide pore region. The pore size in this region would be reduced based on the chain length of the silanes. Before the wide pore region was filled, further deposition of silane molecules did not cause any change in the pore size.

A step growth was proposed to explain the step change in pore sizes as shown in Figure 12. Initially, the silane molecules were deposited in the wide pore region and reduced the pore radii in this region by a number corresponding to the chain length (about 7−8 Å) (a and b). No deposition occurred in the narrow pore region. After the wide pore region was filled, the molecules began to deposit in the narrow pore region, reducing the pore radii in this region by about 5 Å (c). Up to this stage, the pore size in the wide pore region did not decrease further. In this process, the layer thickness in the narrow pore region (5 Å) was less than the expected chain length, indicating that the packing in these regions was not efficient. This result was expected due to the positive surface curvature in these regions. When the surfaces in the narrow pore region were filled, a second layer began to deposit in the wide pore region and reduced the pore radii in this region by another 7 Å (roughly corresponding to the chain length) (d). These results also suggested that the deposition did not stop at the second layer. However, the third layer was not oriented, and the thickness was only about 3 Å.

Multifunctional Molecular Structures: Toward "Biomimic" and "Enzyme Mimic" Nanoporous Materials

So far, the properties and the applications of simple molecular layers have been discussed. These molecular structures involve one or two functional groups and perform mostly one function, such as adsorption.[35,36] Nature has numerous examples in which materials not only exhibit nanoscale ordering, but also contain a multiple of functional molecules perfectly arranged to perform

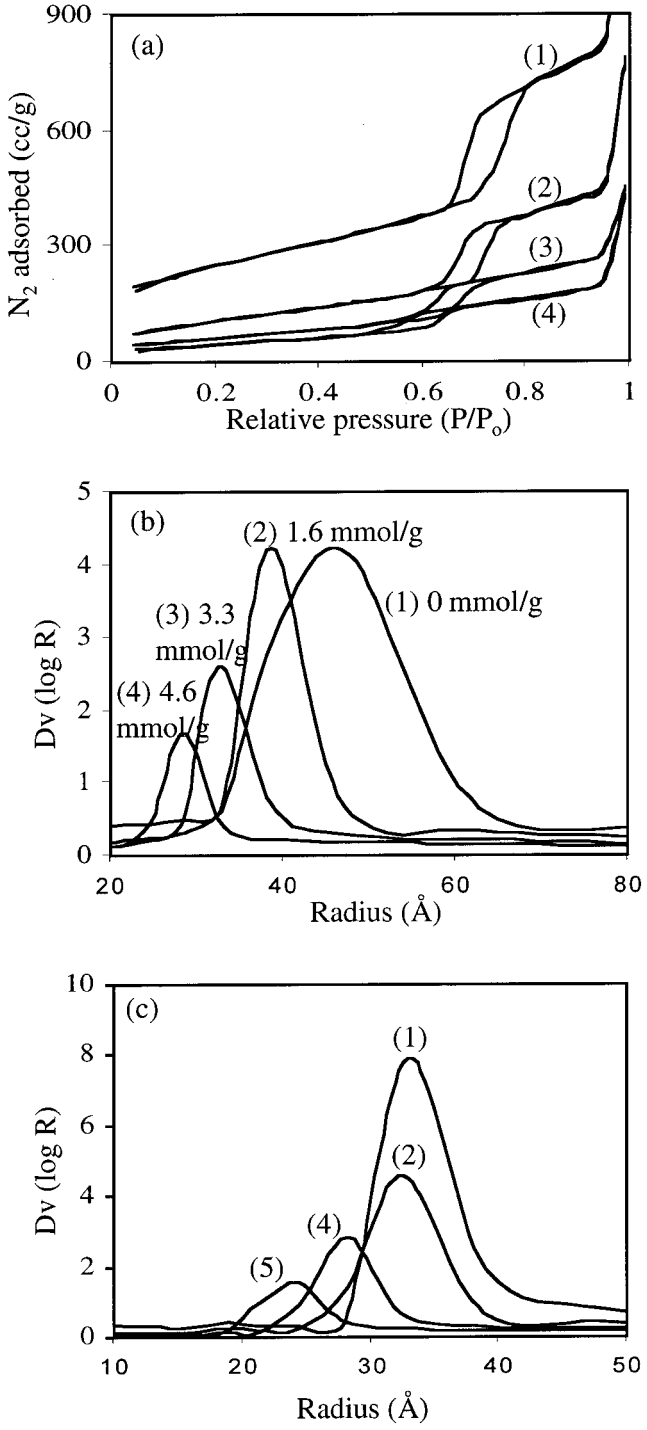

Figure 11. Stepwise change in the pore size, as reflected in the N_2 adsorption isotherm, and the pore-size distribution. (a) N_2 adsorption isotherms with different surface coverage of APS: (1) no APS, (2) 1.6 mmol APS/g silica, (3) 3.3 mmol APS/g silica, (4) 4.6 mmol APS/g silica. (b) Pore-size distributions from the adsorption branch. (c) Pore-size distributions from the desorption branch: (1) no APS, (2) 1.6 mmol APS/g silica, (4) 4.6 mmol APS/g silica, (5) 5.7 mmol APS/g silica.

a wide range of biological functions simultaneously, such as sensing, catalysis, size and shape selection, and response. We are especially inspired by two examples. The first example is an enzyme. An enzyme is one of the most effective catalysts in nature.[56] An enzyme-catalyzed reaction is usually very specific and very rapid, even under mild reaction conditions. The activity of an enzyme is related to the many functional groups on the surface and how they are spatially distributed. In synthetic catalysis, usually only one functional group is involved. Another

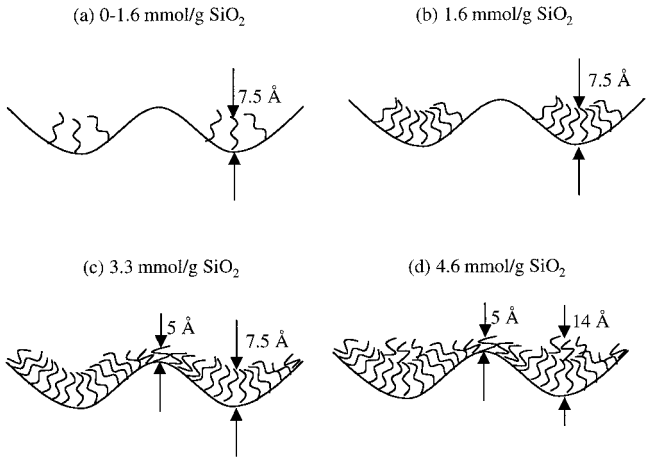

Figure 12. A stepwise growth mechanism for monolayer formation.

example is the selective transport and separation performed by soft lipid membranes.[57] These membranes contain microporous channels and pores. Biological systems self-regulate materials transport through conformational changes of membrane proteins that precisely control the ion and molecular permeability across the membrane surfaces. The precise nature of the selectivity and the self-regulated process are unmatched in man-made materials. In industrial processes, microporous zeolites with well-defined cage structures are used for size selectivity.[58] These materials are made of three-dimensional crystalline frameworks containing interpenetrating pore channels, usually less than 10 Å in size. A change in the synthetic conditions, including temperature, pressure, precursor materials, ionic strength, or "templating" cations, will lead to different microporous materials.

Considerable efforts have been directed to the preparation of enzyme mimic polymers. For example, chymotrypsin is widely studied for the hydrolyses of esters and peptides.[59,60] Chymotrypsin is a well-known hydrolytic enzyme used in amino acid sequential analysis of polypeptides by hydrolyzing specific peptides.[61] This enzyme preferentially hydrolyzes the carboxyl group of the peptide bonds with the aromatic side chains, such as phenylalanine, tyrosin, and tryptophan, and of large hydrophobic residues, such as methionine. It also has esterase activity as in the case of nitrophenyl acetate, which plays an important role in chemical synthesis, and has a close relationship to peptide bonds. The active site of chymotrypsin is known to be the triad, Asp-102, His-57, and Ser-195, sharing a proton-transfer mechanism and effectively catalyzing the reaction of the substrate. This reaction involves hydroxyl, amine, imidazole, and carboxylate groups. Besides, the hydrophobic pocket plays a crucial role in deciding the specific substrate.

Currently, it is impossible to simulate the structure and the functions of an enzyme. However, we have demonstrated that the nanoporous channels can be used as a "nanofactory" to assemble the multifunctional groups and provide catalytic activities that are absent if only individual functional groups are used. We synthesized a multifunctionalized mesoporous material containing five different functional groups, isobutyl, diol, ethylenediamine, dihydroimidazole, and carboxylate. This material is used as a catalyst for rapid hydrolysis of the phenyl ester.[62] The reaction rates and the derived Michaelis constants are shown in Table 3. The reaction rates, as well as the Michaelis constants, are within the range of chymotypsin catalyzed hydrolysis.[63] We also found that all these five groups were required for enhanced catalytic activity toward the hydrolysis of esters. An optimum amount of hydrophobic isobutyl groups

TABLE 3: The Properties and the Biophysical Constants for Hydrolysis of Phenyl Ester[a]

amount of functionalized silanes added[b] (mol % of total silane)	amount of isobutyl group added (mol % of total silane)	PANA (μM)	initial rate (v_0, μM/min)	K_m (μM)	V_{max} (μM/mg/min)
16	0	100	4.956	421	0.18
16	0	200	9.910		
16	0	300	11.201		
16	0	400	11.266		
16	4	100	9.941	57	0.10
16	4	200	10.673		
16	4	300	12.799		
16	4	400	12.887		
16	12	100	39.734	978	2.85
16	12	200	69.675		
16	12	300	110.542		
16	12	400	118.030		
16	24	100	7.304	317	0.21
16	24	200	13.493		
16	24	300	13.444		
16	24	400	17.571		

[a]Conditions for the reactions were given in ref 62. [b] Functionalized silanes include 4% 5,6-dihydroxyhexyl-, 4% carboxyethyl-, 4% dihydroimidazolepropyl-, and 4% *N*-aminoethylaminopropylsilane. The reaction rates are fitted with a Michaelis−Menten equation. PANA represents the reactant, *p*-nitrophenylacetate. v_o is the initial reaction velocity (rate), V_{Max} is the maximum velocity, and K_m Michaelis−Menten constant.

(12%) increases the reaction rate by an order of magnitude. Although ester hydrolysis is not a difficult reaction, this simple and flexible approach allows us to adjust the multifunctionality on the nanometer scale, an essential requirement in preparing "enzyme-like" catalysts.

The multifunctionalized nanoporous materials are still very primitive. The role of each individual group has not been understood yet. True enzyme-like properties for biological agents such as polypeptides have yet to be demonstrated. For example, biological activity is mostly related to how the multifunctional molecules are arranged in three dimensions on several length scales. The three-dimensional arrangement is difficult to achieve using the one-step assembly approach we discussed so far.

To control the three-dimensional architecture, a new multistep assembly approach[64] was developed, based on a molecular imprinting technique. This approach also created a novel hierarchical porous material with tunable size and shape selective pore structures to mimic the microchannels in biomembranes. Soft molecular coatings were introduced with embedded microcavities. This material contains a rigid mesoporous oxide frame, coated by a soft, "microporous" molecular monolayer, as schematically shown in Figure 13. Unlike in zeolite-based materials, the size and shape selectivity is not determined by the oxide framework but by the long-chain molecular monolayers.

The synthetic method is similar to the lithography technique used in the microelectronic industry. It can be called "molecular lithography" because of the small scales used. By properly choosing the template molecules, the size and shape of the cavities can be systematically varied. Zeolite-like properties, such as size and shape selective adsorption and selective catalysis, have been demonstrated. In addition, we can take advantage of the conformational changes of the long-chain molecules in the monolayer coating to regulate the accessibility of the microporous cavities in the monolayer. Tunable access is a highly sought-after property and is usually observed in biomembranes, but not in inorganic microporous materials. The

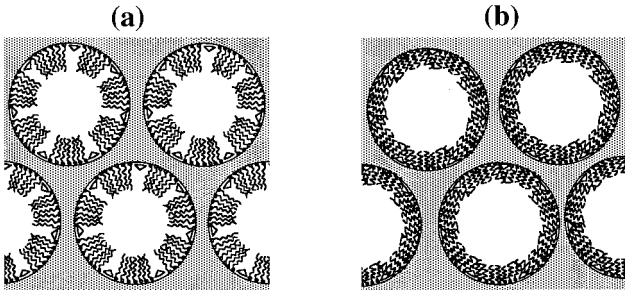

Figure 13. Schematic of the hierarchical porous materials with ordered mesoporosities and microcavities in the long-chain molecular monolayer coatings. The triangular shape in the cavity represents the template molecules, or the idealized shape of the cavity. (a) The porosity in an open position. (b) The porosity in a closed position. Reprinted with permission from ref 64. Copyright 2000 Wiley−VCH.

microcavities are fully accessible in the open position and partially accessible or inaccessible in the closed position.

The molecular lithography process, as shown in Figure 14, was developed from widely investigated molecular imprinting techniques[65] and involves the formation of heterogeneous, multifunctional molecular monolayers. Nominally triangular (tripods), linear (dipods), and point cavities were created by first bonding short 3-aminopropyltrimethoxysilanes (APS) to the template molecules, followed by the deposition of the template-bound silanes onto the mesoporous substrate. The tripod chemistry on silica substrates was first reported by Tahmassebi et al.[66] Subsequently, long-chain molecules were deposited on unoccupied surface of the silica substrates. The template molecules were selectively removed from the substrates with a mild acid wash to leave the desired cavities in the monolayer coating. More details of the procedure are included in ref 67 as well as in a separate publication.[64]

The molecular chain conformations have been studied using N_2 adsorption and NMR techniques during each step of the imprinting process. The layer thickness derived from the pore-size change is consistent with the expected chain length and chain conformation. The surface area in each step was reduced, depending on the amount of organic silanes added and on the final pore size. Ideally, the imprinting procedure should produce triangular cavities (10 Å wide, based on the dimension of the template) and linear cavities (10 Å long). For point cavities, APS molecules were first deposited on the porous substrate, followed by the deposition of octadecyltrimethoxysilane (OTS). The dimension of the point cavities was determined from the area an APS molecule would occupy (about 4.5 Å for one point cavity) on the surface.

The microcavities on the monolayer coatings showed considerable selectivity during adsorption studies.[68] The adsorption results of tripod molecules on different substrates are plotted in Figure 15a. Similar results were also obtained with dipod molecules (Figure 15b). Considering the fact that the difference between the tripod and dipod molecules is not great, the capability of the substrate to differentiate between these two molecules is remarkable. A tripod molecule has three benzaldehyde arms, and a dipod has two. The rest of the molecular structures are similar. In principle, the dipod molecules can easily fit into the triangular cavities and conform to the majority of the cavities nicely. The two aldehyde groups can also bind with the two amine groups at the corner of the cavity (hydrogen bonding or forming Schiff base). We would expect the dipod molecules to adsorb on triangular cavities as well as the linear cavities. The large difference in the adsorption behavior of dipod molecules on triangular and linear cavities demonstrated that the shapes of the cavities are very important.

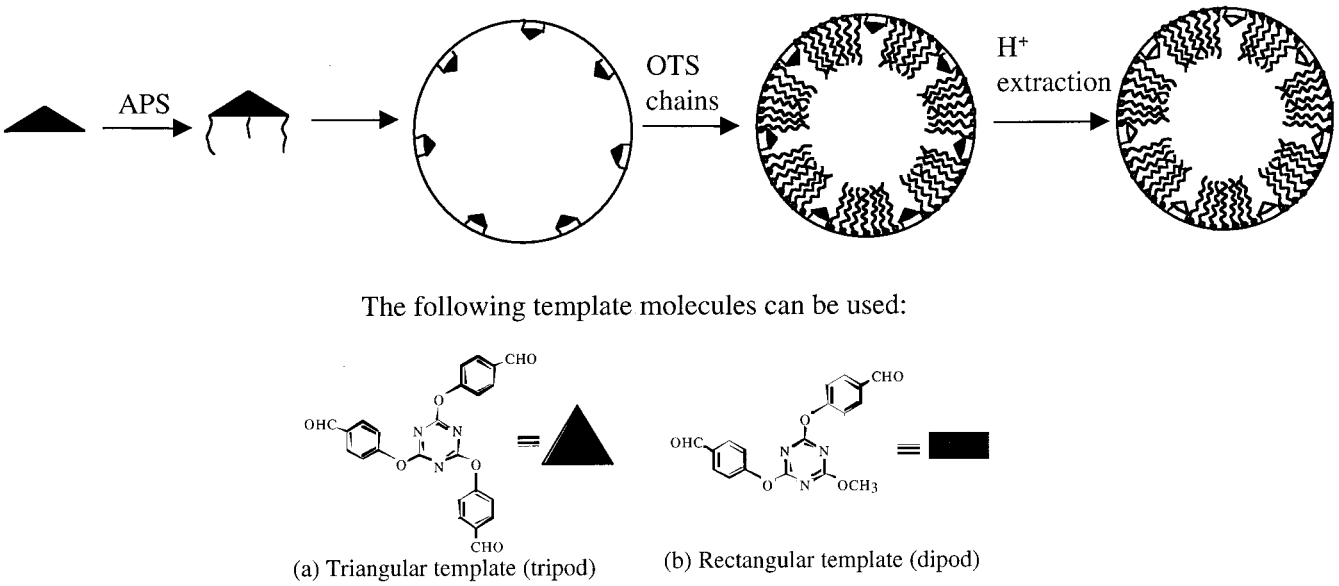

Figure 14. Schematics of the molecular imprinting process.

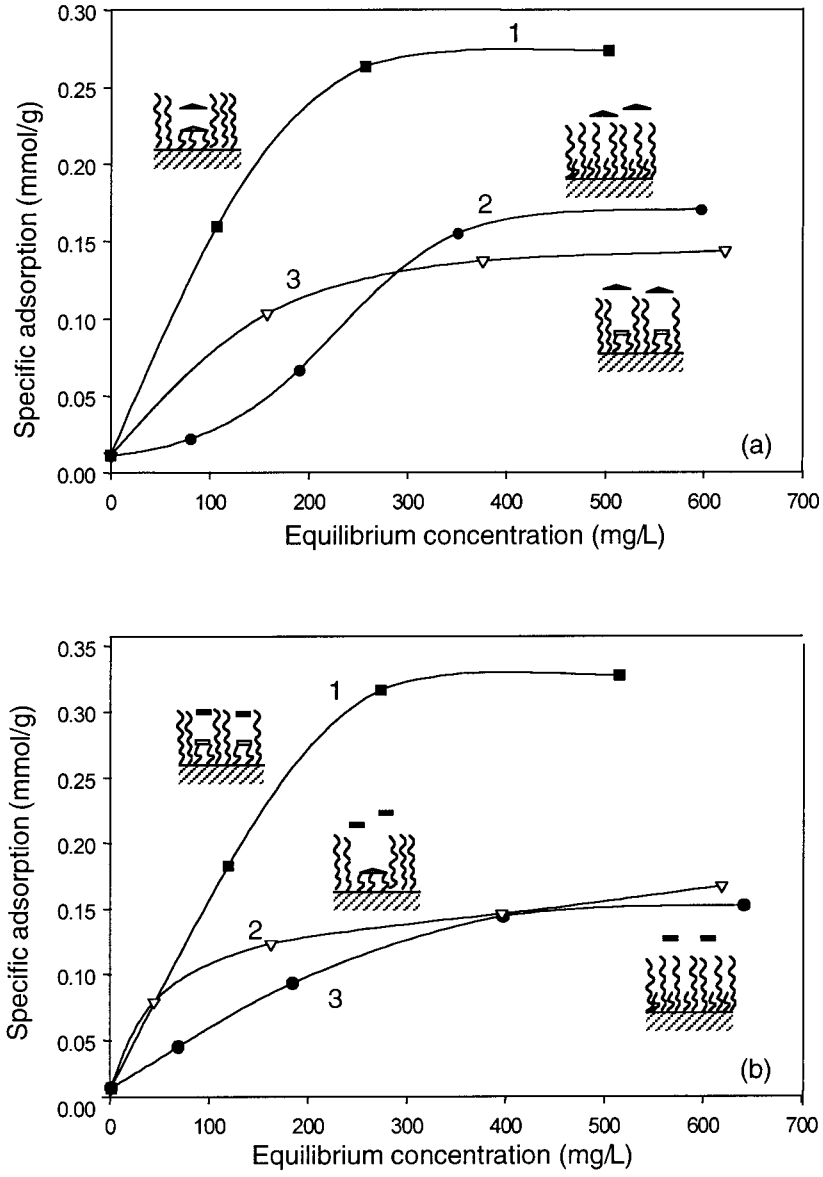

Figure 15. Adsorption results of (a) tripod molecules and (b) dipod molecules. (1) Triangular cavities, (2) linear cavities, and (3) point cavities. Reprinted with permission from ref 69. Copyright 2000 Wiley-VCH.

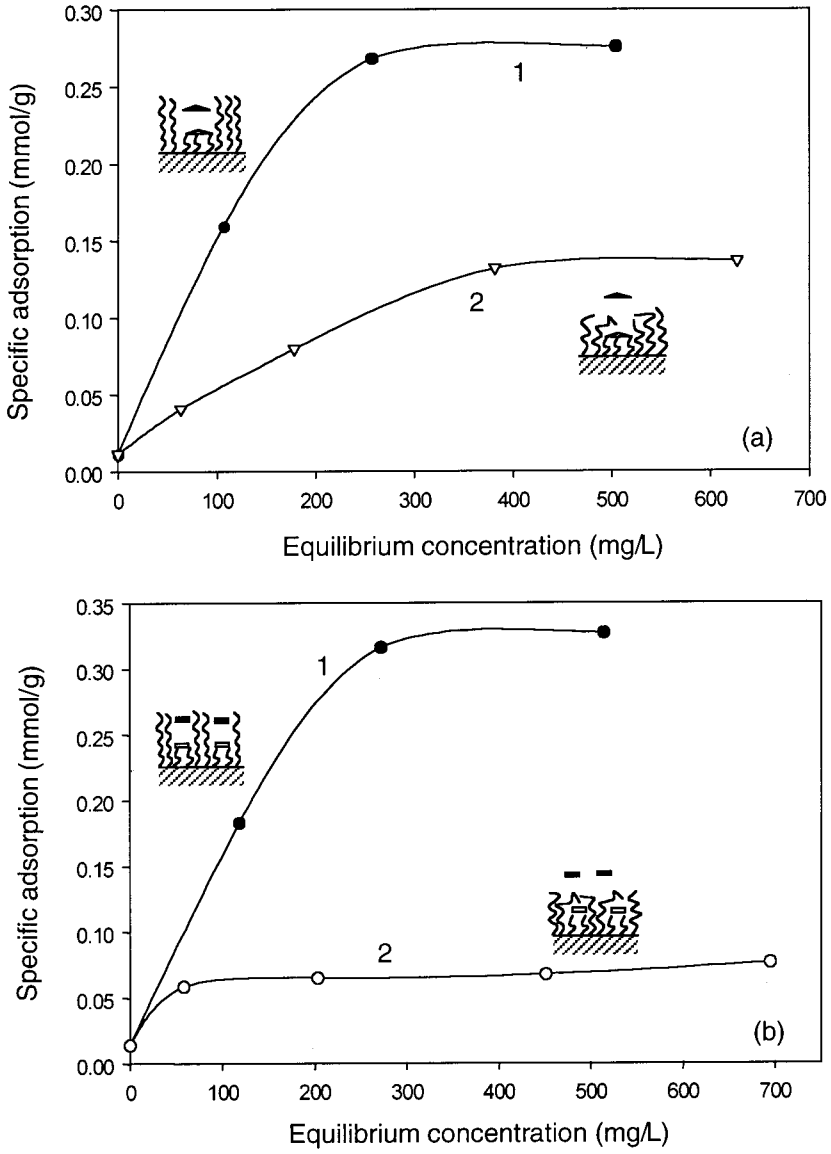

Figure 16. Solvent effects on adsorption behavior (reprinted with permission from ref 64. Copyright 2000 Wiley-VCH). (a) Tripod molecules on triangular cavities: (1) in toluene and (2) in toluene/ethanol. (b) Dipod molecules on linear cavities: (1) in toluene and (2) in toluene/ethanol.

The selectivity of the microcavities is directly related to the three-dimensional nature of the long-chain molecule coatings. Merely one-to-one correspondence of the binding sites does not give any selectivity. Materials have been prepared using the same procedure without the long-chain molecule monolayer coating or with a coating layer made of small molecules (hexamethyl disilazane or trimethoxypropylsilane (TMPS)). These materials contain exactly the same bindings sites (amine groups from the APS) arranged the same way as in the long-chain monolayers. No selectivity was observed on any of these materials without the long-chain capping. If the selectivity were solely attributed to the matching of the binding sites, the materials without capping or with the short-chain capping layer should have similar selectivity as the long-chain materials. Therefore, we can conclude that the steric effect of the cavities in the long-chain monolayers largely contributed to the selectivity of such materials.

One of the most important properties of the new material is that the accessibility of the microcavities can be changed. This property is demonstrated with adsorption studies conducted in mixed solutions of toluene and ethanol.[69] Generally, whether the long-chain molecules assume an extended or a collapsed conformation depends on the inter- and intramolecular forces. Toluene and the surface bound long-chain hydrocarbons are both hydrophobic molecules and have a similar dielectric constant (ϵ) and refractive index (n) ($\epsilon_{\text{toluene}} \approx 2.37$, $\epsilon_{\text{C18}} \approx 2.0$, $n_{\text{toluene}} \approx 1.49$, $n_{\text{C18}} \approx 1.44$). The interactions within and between the long hydrocarbon chains in toluene are greatly reduced.[70] Therefore, these hydrocarbon chains will assume a more extended conformation, making the microcavities accessible.

However, ethanol is a hydrophilic solvent and has a different dielectric constant and refractive index ($\epsilon_{\text{EtOH}} \approx 26$, $n_{\text{EtOH}} \approx 1.36$). In a solvent containing ethanol, the attractive forces within and between the long hydrocarbon chains increase.[70] This will cause the hydrocarbon chains to form a more compact (collapsed) conformation, blocking the microcavities from molecules in the solvent. This kind of molecular conformation change, when the solvency of the solution is changed, is well documented in textbooks.[71] Figure 16a compares the results of tripod adsorption on triangular cavities in toluene and in a toluene/ethanol (1:1 ratio by volume) mixture. The adsorption in the mixture is greatly reduced. It is interesting to compare Figure 16a with Figure 16b (dipod adsorption on linear cavities). In Figure 16b, the adsorption in the mixture was nearly shut off. The linear cavities are much narrower than the triangular

cavities. When the hydrocarbon chains curl over, the accessibility to the linear cavities can be completely shut off.

We have also shown that size-selective catalytic reactions can be performed using Knoevenagel condensation between malononitrile and benzaldehyde or 3-pentanone as an example.[72,73] The use of amino groups immobilized on silica as a weak base catalyst for Knoevenagel condensation was reported by Angeletti et al.[74] and by others.[75] Several reaction pathways have been discussed.[64−76] Although the detailed reaction pathways need to be further illustrated, we have shown that we can selectively enhance or reduce the reaction rate by manipulating the monolayer chemistry and the geometry of the cavities. The large cavities (triangular and linear) give a higher yield than the point cavities for the condensation between malononitrile and benzaldehyde. The relative difference between the triangular and point cavities ranges from 30% to 70%.

Conclusions

We have shown in this paper, as well as in the publications referenced in this paper, that assembly of molecular structures in ordered mesoporosity has produced a range of useful nanoscale materials. The capability to manipulate the surface and interfacial chemistry on the nanometer scale with multifunctional molecules and groups will lead to much more sophisticated materials, with properties approaching that of the biological counterparts, such as enzymes, and biological membranes.

The molecular assembly process and the molecular conformations are sensitive to the pore structure and pore size. The molecular layers in 10 nm pores are more homogeneous than those in 3 nm, 17 nm, and 30 nm pores. In addition, hydrocarbon chains of intermediate length (C10) tend to form better monolayers than short chains and very long chains in the mesoporosity. The ordered mesoporosity also provides an ideal medium to study the accessibiliy of model molecules in the pore channels and provides new atomistic insights for understanding monolayer chemistry. For example, for the first time, the deposition of the monolayers was found to be stepwise, depending on the surface roughness. Strictly speaking, single-layer monolayer coatings are difficult to achieve as long as the surface coverage is reasonably high.

The stepwise growth model has some implications on the properties of the materials. We can easily speculate that when molecules are deposited, rather than being uniformly distributed on the surface, dimers, trimers, or even high-order clusters could form. The aggregation of these molecules on the surface would have a negative effect on the selectivity, based on the size and shape of the cavities. The possibility also exists of forming more than one molecular layer, or aggregation of the monolayer molecules. We still need to understand to what degree these aggregation phenomena will affect the properties (such as selectivity), or if we can even take advantage of the stepwise growth to form multiscale molecular coatings.

Acknowledgment. Pacific Northwest National Laboratory is operated by Battelle for the U. S. Department of Energy under Contract DE-AC06-76RL0 1830. This work is supported by the Office of Basic Energy Sciences, Division of Materials Sciences, of the U.S. Department of Energy. We also acknowledge editorial assistance from Susan G. McGuire, who also provided valuable technical suggestions. The figure on the cover page is based on computer modeling performed by Dr. Kim Ferris of the Pacific Northwest National Laboratory.

References and Notes

(1) (a) Beck, J. S.; Vartuli, J. C.; Roth, W. J.; Leonowicz, M. E.; Kresge, C. T.; Schmitt, K. D.; Chu, C. T−W.; Olson, D. H.; Sheppard, E. W.; McCullen, S. B.; Higgins, J. B.; Schlenker, J. L. *J. Am. Chem. Soc.* **1992**, *114*, 10834. (b) Kresge, C. T.; Leonowicz, M. E.; Roth, W. J.; Vartuli, J. C.; Beck, J. S. *Nature* **1992**, *359*, 710.

(2) Monnier, A.; Schüth, F.; Huo, Q.; Kumar, D.; Margolese, D.; Maxwell, R. S.; Stucky, G. D.; Krishnamurty, M.; Petroff, P.; Firouzi, A.; Janicke, M.; Chmelka, B. F. *Science* **1993**, *261*, 1299.

(3) For reviews, see: (a) Beck, J. S.; Vartuli, J. C. *Curr. Opin. Solid State Mater. Sci.* **1996**, *1*, 76. (b) Liu, J.; Kim, A. Y.; Wang, L.-Q.; Palmer, B. J.; Chen, Y. L.; Bruinsma, P.; Bunker, B. C.; Exarhos, G. J.; Graff, G. L.; Rieke, P. C.; Fryxell, G. E.; Virden, J. W.; Tarasevich, B. J.; Chick. L. A. *Adv. Colloid Interface Sci.* **1996**, *69*, 131. (c) Raman, N. K.; Anderson, M. T.; Brinker, C. J. *Chem. Mater.* **1996**, *8*, 1682. (d) Zhao, D.; Yang, P.; Hua, Q.; Chmelka, B. F.; Stucky, G. D. *Curr. Opin. Solid State Mater. Sci.* **1998**, *3*, 121.

(4) (a) Vandry, F.; Khodabandeh, S.; Davis, M. E. *Chem. Mater.* **1996**, *8*, 1451. (b) Bagshaw, B. A.; Pinnavia, T. J. *Angew. Chem., Int. Ed. Engl.* **1996**, *35*, 1102. (c) Knowles, J. A.; Hudson, M. J. *J. Chem. Soc., Chem. Commun.* **1995**, 2083. (d) Schmidt, R.; Akporiaye, D.; Stöcker, M.; Ellestad, O. H. *J. Chem. Soc., Chem. Commun.* **1994**, 1493. (e) Antonelli, D. M.; Ying, J. Y. *Chem. Mater.* **1996**, **8**, 874. (f) Antonelli, D. M.; Ying, J. Y. *Angew. Chem., Int. Ed. Engl.* **1995**, *34*, 4, 2014.

(5) Tian, Z.-R.; Tong, W.; Wang, J.-Y.; Duan, N.-G.; Krishnan, V. V.; Suib, S. L. *Science* **1997**, *276*, 926.

(6) Attard, G. S.; Barlett, P. N.; Coleman, N. R. B.; Elliott, J. M.; Owen, J. R.; Wang, J. H. *Science* **1997**, *278*, 838.

(7) Huo, Q.; Margolese, D. I.; Ciesla, U.; Feng, P.; Gier, T. E.; Sieger, P.; Leon, R.; Petroff, P. M.; Schüth, F.; Stucky, G. D. *Nature* **1994**, *368*, 317.

(8) Tanev, P. T.; Pinnavaia, T. J. *Science* **1995**, *267*, 865.

(9) Bagshaw, S. A.; Prouzet, E.; Pinnavia, T. J. *Science* **1995**, *267*, 865.

(10) MacLachlan, M. J.; Coombs, N.; Ozin, G. A. *Nature* **1999**, *397*, 681.

(11) Zhao, D.; Feng, J.; Huo, Q.; Melosh, N.; Fredrickson, G. H.; Chmelka, B. F.; Stucky, G. D. *Science* **1998**, *279*, 548.

(12) Yang, P.; Zhao, D.; Margolese, D. I.; Chmelka, B. F.; Stucky, G. D. *Nature* **1998**, *396*, 152.

(13) Yang, H.; Kuperman, A.; Coombs, N.; Mamiche-Afrara, S.; Ozin, G. A. *Nature* **1996**, *379*, 703.

(14) Aksay, I. A.; Trau, M.; Manne, S.; Honma, I.; Yao, N.; Zhou, L.; Fenter, P.; Eisenberger, P. M.; Gruner, S. M. *Science* **1996**, *273*, 892.

(15) Yang, H.; Coombs, N.; Sokolov, I.; Ozin, G. A. *Nature* **1996**, *381*, 589.

(16) Hua, Q.; Feng, J.; Schüth, F.; Stucky, G. D. *Chem. Mater.* **1997**, *9*, 14.

(17) Lu, Y.; Fan, H.; Stump, A.; Ward, T. L.; Rieker, T.; Brinker, C. F. *Nature* **1999**, *398*, 223.

(18) Bruinsma, P. J.; Kim, A. Y.; Liu, J.; Baskaran, S. *Chem. Mater.* **1998**, *10*, 2507.

(19) Yang, P.; Zhao, D.; Chmelka, B. F.; Stucky, G. D. *Chem. Mater.* **1998**, *10*, 2033.

(20) Antonelli, D. M.; Nakahira, A.; Ying, J. Y. *Inorg. Chem.* **1996**, *35*, 3126.

(21) Lu, Y.; Gangull, R.; Drewien, C. A.; Anderson, M. T.; Brinker, C. F.; Gong, W.; Guo, Y.; Soyez, H.; Dunn, B.; Huang, M. H.; Zink, J. I. *Nature* **1997**, *389*, 364.

(22) Zhao, D.; Yang, P.; Melosh, N.; Feng, J.; Chmelka, B. F.; Stucky, G. D. *Adv. Mater.* **1997**, *9*, 1380.

(23) Baskaran, S.; Liu, J.; Domansky, K.; Kohler, N.; Li, X.; Coyle, C.; Fryxell, G. E.; Thevathasan, S.; Williford, R. E. *Adv. Mater.* **2000**, 12, 291.

(24) Tolbert, S. H.; Firouzi, A.; Stucky, G. D.; Chmelka, B. F. *Science* **1997**, *278*, 264.

(25) Yang, H.; Coombs, N.; Ozin, G. A. *Nature* **1997**, *386*, 692.

(26) Kim, S. S.; Zhang, W.; Pinnavaia, T. J. *Science* **1998**, *282*, 1302.

(27) Yang, P.; Deng, T.; Zhao, D.; Feng, J.; Pine, D.; Chmelka, B. F.; Whitesides, G. M.; Stucky, G. D. *Science* **1998**, *282*, 2244.

(28) Yang, P.; Wirnberger, G.; Huang, H. C.; Cordero, S. R.; McGehee, M D.; Scott, B.; Deng, T.; Whitesides, G. M.; Chmelka, B. F.; Buratto, S. K.; Stucky, G. D. *Science* **2000**, *287*, 465.

(29) Cha, J. N.; Stucky, G. D.; Morse, D. E.; Deming, T. J. *Nature* **2000**, *403*, 289.

(30) Tanev, P. T.; Chibwe, M.; Pinnavaia, T. J. *Nature* **1994**, *368*, 6469.

(31) Wu, C. H.; Bein, T. *Science* **1994**, *264*, 5166.

(32) Zhou, W.; Thomas, J. M.; Shephard, D. S.; Johnson, B. F. G.; Ozkaya, D.; Maschmeyer, T.; Bell, R. G.; Ge, Q. *Science* **1998**, *280*, 705.

(33) Kageyama, K.; Tamazawa, J.-I.; Aida, T. *Science* **1999**, *285*, 2113.

(34) (a) Inagaki, S. *J. Am. Chem. Soc.* **1999**, *121*, 9611. (b) Stein, A. *Chem. Mater.* **1999**, *11*, 3302. (c) Asefa, T.; MacLachlan, M. J.; Coombs, N.; Ozin, G. A. *Nature* **1999**, *402*, 867.

(35) (a) Mercier, L.; Pinnavaia, T. J. *Adv. Mater.* **1997**, *9*, 500. (b) Mercier, L.; Pinnavaia, T. J. *Environ. Sci. Technol.* **1998**, *32*, 2749.

(36) (a) Feng, X.; Fryxell, G. E.; Wang, L.-Q.; Kim, A. Y.; Kemner, K.; Liu, J. *Science* **1997**, *276*, 923. (b) Liu, J.; Feng, X.; Fryxell, G. E.; Wang, L.-Q.; Kim, A. Y.; Gong, M. *Adv. Mater.* **1998**, *10*, 161.

(37) Fryxell, G. E.; Liu, J.; Hauser, T. A.; Nie, Z.; Ferris, K. F. *Chem. Mater.* **1999**, *11*, 2148.

(38) Feng, X.; Rao, L.; Mohs, T. R.; Xu, J.; Xia, Y.; Fryxell, G. E.; Liu, J.; Raymond, K. N. Self-assembled Monolayers on Mesoporous Silica, a Super Sponge for Actinides. In *Ceramic Transactions, Environmental Issues and Waste Management Technologies IV*, Mara, J. C., Chandler, G. T., Ed.; American Ceramic Society: Westerville, OH, 1999; Vol. 93, pp 35−42.

(39) Sayari, A. *Chem. Mater.* **1996**, *8*, 1840.

(40) Möller, K.; Bein, T. *Chem. Mater.* **1998**, *10*, 2950.

(41) Cauvel, D.; Renard, G.; Brunel, D. *J. Org. Chem.* **1997**, *62*, 749.

(42) Burkett, S. L.; Simms, S. D.; Mann, S. *J. Chem. Soc., Chem. Commun.* **1996**, 1367.

(43) Lim, M. H.; Blanford, C. F.; Stein, A. *Chem. Mater.* **1998**, *10*, 467.

(44) (a) Whitesides, G. M. *Sci. Am.* **1995**, *273*, 146. (b) Ulman, A. *Chem. Rev.* **1996**, *96*, 1533.

(45) Bunker, B. C.; Rieke, P. C.; Tarasevich, B. J.; Campbell, A. A.; Fryxell, G. E.; Graff, G. L.; Song, L.; Liu, J.; Virden, J. W.; McVay, G. L. *Science* **1994**, *264*, 48.

(46) Linsen, B. G.; van den Heuvel, A. *The Solid Gas Interface*; Flood, E. A., Ed.; Mercel Dekker: New York, 1967; Vol. 2, p 1025.

(47) Kruk, M.; Jaroniec, M.; Sayari, A. *Langmiur* **1997**, *13*, 6267.

(48) Kruk, M.; Jaroniec, M.; Sakamoto, Y.; Terasaki, O.; Ryoo, R.; Ko, C. H. *J. Phy. Chem. B* **2000**, *104*, 292.

(49) Antochshuk, V.; Jaroniec, M. *J. Phys. Chem. B* **1999**, *103*, 6252.

(50) Fatumbi, H. O.; Bruch, M. D.; Wirth, M. J. *Anal. Chem.* **1993**, *65*, 2048.

(51) The 75.0 MHz ^{13}C and ^{29}Si solid-state NMR experiments were carried out with a Chemagnetics spectrometer (300 MHz, 89-mm wide-bore Oxford magnet) using a variable-temperature double-resonance probe. The dried samples were loaded into 7-mm Zirconia PENCIL rotors and spun at 3−4 kHz. For all experiments, 40-ms acquisition times and a 50-KHz spectral window were employed. The number of transients was 500−5000. For NMR experiments, both single-pulse (SP) Bloch-decay and cross-polarization (CP) methods were used with ^{1}H decoupling. SP spectra were collected using a 4.5 μs (90°) ^{13}C pulse and a 10-s repetition delay. The power levels of the carbon and proton channels were set so that the Hartmann−Hahn match was achieved at 55 kHz in CP experiments. A Lorentzian line broadening of 4 Hz was used for all ^{13}C (SP) spectra. The ^{13}C chemical shifts were referenced to tetramethylsilane (TMS) at 0 ppm. For NMR analysis of ^{29}Si, spectra were collected by using a single-pulse Bloch-decay method (with proton decoupling) with a 5-μs (90°) ^{29}Si pulse, and a 30-s repetition delay. A Lorentzian line broadening of 50 Hz was used for all ^{29}Si (SP) spectra. The ^{29}Si chemical shift was referenced to TMS.

(52) Rassing, J.; McKenna, W. P.; Bandyopadhyay, S.; Eyring, E. M. *J. Mol. Liq.* **1984**, *27*, 165.

(53) Bierbaum, K.; Kinzler, M.; Woll, C. H.; Grunze, M. *Langmiur* **1995**, *11*, 512.

(54) Maoz, R.; Sagiv, J. *J. Colloid Interface Sci.* **1984**, *100*, 465.

(55) Schwartz, D. K.; Steinberg, S.; Israelachvili, J.; Zasadzinski, J. A. N. *Phys. Rev. Lett.* **1992**, *69*, 334.

(56) Zubay, G. L. *Biochemistry*, 4th ed.; William. C. Brown: Dubuque, IA, 1998; pp 159−176.

(57) Gennis, R. B. *Biomembranes, Molecular Structure and Function*, Springer-Verlag: New York, 1989; Chapter 8, pp 270−322.

(58) (a) Barrer, R. M. *Hydrothermal Chemistry of Zeolites*; Academic Press: New York, 1982. (b) Davis, M. E. *Ind. Eng. Chem. Res.* **1991**, *30*, 1675. (c) Ribeiro, F. R.; Alvarez, F.; Henriques, C.; Lemos, F.; Lopes, J. M.; Ribeiro, M. F. *J. Mol. Catal. A: Chem.* **1995**, *96*, 245.

(59) (a) Kunitake, T.; Okahata, Y. *J. Am. Chem. Soc.* **1976**, *98*, 7793. (b) Kunitake, T.; Okahata, Y.; Sakamoto, T. *J. Am. Chem. Soc.* **1976**, *98*, 7799. (c) Kunitake, T.; Okahata, Y. *Macromolecules* **1976**, *9*, 15. (d) Kunitake, T.; Horie, S. *Bull. Chem. Soc. Jpn.* **1975**, *48*, 1304.

(60) Lawin, L. R.; Fife, W. K.; Tian, C. X. *Langmuir* **2000**, *16*, 3583.

(61) (a) Blow, D. M. *Acc. Chem. Res.*, **1976**, *9*, 145. (b) Bender, M. L.; Kezdy, F. J. *J. Am. Chem. Soc.* **1964**, *86*, 3704.

(62) The hydrolysis of *p*-nitrophenylacetate (PNPA) to *p*-nitrophenol was studied in 0.1 M tris-HCl buffer (pH = 7.6) solutions. The kinetic products were measured on UV−vis spectrophotometer (on a HP 8453 UV−visible Spectrophotometer) (PNPA: 273 nm. *p*-nitrophenol: 400 nm.) after the solution was filtered using a 0.2 uM syringe filter. The amount of *p*-nitrophenol released was calibrated by known concentration of pure *p*-nitrophenol.

(63) (a) Blow, D. M. *Acc. Chem. Res.* **1976**, *9*, 145. (b) Bender, M. L.; Kezdy, F. J. *J. Am. Chem. Soc.* **1964**, *86*, 3704.

(64) Shin, Y.; Liu, J.; Wang, L.-Q.; Nie, Z.; Samuels, W. D.; Fryxell, G. E.; Exarhos, G. J. *Angew. Chem., Int. Ed. Engl.* **2000**. In press.

(65) For a review, see: (a) Wulf, G. *Angew Chem., Int. Ed. Engl.* **1995**, *34*, 1812. (b) Davis, M. E.; Katz, A.; Ahmad, W. R. *Chem. Mater.* **1996**, *8*, 1820.

(66) Tahmassebi, D. C.; Sasaki, T. *J. Org. Chem.* **1994**, *59*, 679. (b) Hwang, K. O.; Yakura, Y.; Ohuchi, F. S.; Sasaki, T. *Mater. Sci. Eng. C* **1995**, *3*, 137.

(67) The mesoporous silica was prepared according to a method reported in the literature,[1,11] and has a mesoporous silica surface with 517 m^2/g surface area (corrected for microporosity) and 93 Å average pore size. Triangular template molecules (tripod, 2,4,6-tris(*p*-formylphenoxy)-1,3,5-triazine) were synthesized by the reaction of cyanuric chloride with three equivalent moles of *p*-hydroxybenzaldehyde, a procedure first reported by Tahmassebi et al.[62] Linear template molecules (dipod, 2,4-bis(*p*-formylphenoxy)-6-methoxy-1,3,5-triazine) were synthesized by the same procedure using 2,4-dichloro-6-methoxy-1,3,5-triazine instead of cyanuric chloride as a starting material with two equivalent moles of *p*-hydroxybenzaldehyde. The tripod or dipod molecules were then reacted with 3-aminopropyltrimethoxysilane (APS) at room temperature to form tripod-APS or dipod-APS through Schiff bases. This Schiff base was added to a mesoporous silica suspension in toluene and refluxed for 6 h. The tripods should bind to the substrate with a face-on conformation through the amine groups on the three corners, and the dipods should bind to the substrate with an edge-on conformation through the amine groups on the two ends. After 6 h, long-chain organic silanes, such as octadecyltrimethoxysilane (OTS), were added to the solution mixture to form the long-chain molecular monolayer coating. The template molecules were subsequently removed by acid hydrolysis (HCl) of the Schiff bases with aqueous methanol for 4 h.

(68) The adsorption capacity toward dipod or tripod was determined on a HP 8453 UV−Vis spectrophotometer. In all experiments, 0.02 g of each sample was equilibrated with 10.0 mL of different concentration of dipod or tripod in toluene solutions in stoppered glass vials, and these mixtures were stirred for 4 h on the Environ Shaker at room temperature. The difference in the template concentrations before and after equilibration gave the adsorbed amount on the solid samples.

(69) The adsorption study was performed similarly to ref 13, except that a mixture of ethanol and toluene (50:50 by volume) was used as the solvent.

(70) Israelachvili, J. N. *Intermolecular and Surface Forces*, 2nd ed.; Academic Press: San Diego, 1992; p 99.

(71) Billmeyer, F. W., Jr. *Textbook of Polymer Science*, 3rd ed.; John Wiley and Sons: New York, 1984; p 154.

(72) In a typical procedure, 0.05 g of each catalyst and benzaldehyde (0.212 g, 2.0 mmol) were stirred in dry toluene (10.0 mL). To this solution, 0.126 mL (2.0 mmol) of malononitrile was added, and the mixture was stirred at room temperature. The reaction was monitored periodically by UV−Vis spectrophotometer (285 nm for benzaldehyde and 314 nm for product). Similar procedure was used for 3-pentanone, except that the reaction was carried out at 110 °C.

(73) Carey, F. A.; Sundberg, R. J. *Advanced Organic Chemistry B: Reactions and Synthesis*, 2nd ed.; Plenum: New York, 1983; pp 57−59.

(74) Angeletti, E.; Capena, C.; Martinetti, G.; Venturello, P. *J. Chem. Soc., Perkin Trans. I* **1989**, 105.

(75) (a) Choudary, B. M.; Kantam, M. L.; Sreekanth, P.; Bandopadhyay, T.; Figueras, F.; Tuel, A. *J. Mol. Catal. A: Chem.* **1999**, *142*, 361. (b) Rodriguez, I.; Iborra, S.; Corma, A.; Rey, F.; Jorda, J. L. *Chem. Commun.* **1999**, 592.

(76) House, H. O. *Modern Synthetic Reactions*, 2nd ed.; W. A. Benjamin, Inc.: Menlo Park, CA.; 1972; p 648.